A Finite Element Analysis and Circuit Modelling Methodology for Studying Electrical Impedance Myography of Human Limbs

Alejandro Fernandez Schrunder [ID], *Student Member, IEEE*, Saul Rodriguez, *Member, IEEE*, and Ana Rusu [ID], *Member, IEEE*

Abstract—*Objective:* Electrical impedance myography (EIM) measures bioimpedance over muscles. This paper proposes a circuit-based modelling methodology originated from finite element analysis (FEA), to emulate tissues and effects from anthropometric variations, and electrode placements, on EIM measurements. The proposed methodology is demonstrated on the upper arms and lower legs. *Methods:* FEA evaluates impedance spectra (Z-parameters), sensitivity, and volume impedance density for variations of subcutaneous fat thickness (t_f), muscle thickness (t_m), and inter-electrode distance (IED), on limb models over 1Hz-1 MHz frequency range. The limbs' models are based on simplified anatomical data and dielectric properties from published sources. Contributions of tissues to the total impedance are computed from impedance sensitivity and density. FEA Z-parameters are imported into a circuit design environment, and used to develop a three Cole dispersion circuit-based model. FEA and circuit model simulation results are compared with measurements on ten human subjects. *Results:* Muscle contributions are maximized at 31.25 kHz and 62.5 kHz for the upper arm and lower leg, respectively, at 4 cm IED. The circuit model emulates variations in t_f and t_m, and simulates up to 89 times faster than FEA. The circuit model matches subjects measurements with RMS errors $< 36.43\Omega$ and $< 17.28°$, while FEA does with $< 36.59\Omega$ and $< 4.36°$. *Conclusions:* We demonstrate that FEA is able to estimate the optimal frequencies and electrode placements, and circuit-based modelling can accurately emulate the limbs' bioimpedance. *Significance:* The proposed methodology facilitates studying the impact of biophysical principles on EIM, enabling the development of future EIM acquisition systems.

Index Terms—Bioimpedance, muscle, electrical impedance myography, finite element analysis, circuit simulation.

I. INTRODUCTION

ELECTRICAL Impedance Myography (EIM) is a technique that consists in measuring the electrical impedance over a single muscle or group of muscles [1]. EIM is usually performed using 4 surface electrodes placed in a linear array over the muscle of interest, thus minimizing the effect of electrode polarization and impedance on the measurement and maintaining signal quality [1]. The outer electrodes apply a sine-wave current stimulus (AC) in the KHz to MHz frequency range (α and β dispersions). The resulting alternating voltage response from tissues is sensed by the inner electrodes.

EIM has been used as a primary diagnostic tool and disease severity biomarker in a variety of disorders affecting muscles, such as neurogenic disorders, myopathic conditions, muscle atrophy, and traumatic injury of muscle [1], [2]. Recently, EIM has been suggested as a method for reliably detecting muscle contractions [1], [3], [4]. Both single-frequency and multi-frequency EIM have been used to grade the severity of muscular disorders. Nevertheless, multi-frequency EIM provides more information of muscle condition.

As the EIM measurement relies on the flow of current from surface electrodes through multiple tissue layers, the technique is sensitive to both geometrical and electrical factors. For instance, the dielectric properties of biological tissues, anatomy of the body part around the muscle of interest and anatomy of the muscle itself have a considerable effect on the measured impedance. Likewise, the position of electrodes, parallel or perpendicular to the muscle fibers, and the inter-electrode distance (IED) also have an effect on the measurement. In past years, there has been a growing interest to get a deeper understanding of the underlying biophysical mechanisms that affect EIM measurements, allowing to predict outcomes of the measured bioimpedance data. This enables the possibility to develop standards and good practices for using this technique in clinical applications or as a medical research tool. In a similar way, it also enables the possibility to define system specifications for EIM acquisition.

Finite-element analysis (FEA) has been proved to be an effective tool to study biophysical mechanisms in EIM measurements. Previous works on FEA for EIM have performed studies using models based on simplified geometries and dielectric properties of tissues from Gabriel's database [5]–[8]. These works use different geometrical parameters and types of analyses depending on the aim of the study and muscle of interest. In

a previous work [9], FEA was used to analyse how EIM is affected by alterations in the dielectric properties of muscle due to nerve injury. A frequency study over the 0.5KHz-300KHz range, performed on models of the rat hind limbs, accurately predicted the measured 50KHz bioimpedance. Models' geometries were based on MRI data, and muscle's dielectric properties were calculated from measurements on rats before and after nerve injury. This work proved FEA's potential to approximate underlying electrical properties of muscle. However, it did not evaluate the effects of other tissues, anthropometric variations, and electrode arrangements. Therefore, the work was extended in [10] where FEA was used to optimize the IED of a linear electrode array. A frequency study over the 0.5KHz-1MHz range with parametric alterations of subcutaneous fat and muscle thickness was performed on a human arm model. Muscle dielectric properties were taken from [9]. This work had three major findings: (i) reactance is least affected by alterations in subcutaneous fat thickness as compared to resistance and phase; (ii) increasing distance between current injection electrodes reduces the effect of subcutaneous fat and muscle size on the impedance at 35KHz; and (iii) muscle's conductivity has little impact on the 35KHz bioimpedance for variations of distance between current injection electrodes. However, this analysis has only focused on changes of the total impedance, and did not address the contributions of each constituent tissue to the measurement. These contributions and the importance of muscle-specific impedance were considered in [11]. In this work, FEA was used to evaluate tissues' contributions for different electrode arrangements. Frequency and sensitivity distribution studies in the 10KHz-1MHz range, were performed on a model consisting of a planar rectangular slab with 4 layers of tissue (skin, fat, muscle, and bone). These studies also included parametric alterations of subcutaneous fat and IEDs. This work had demonstrated that: (i) there are regions of negative sensitivity, which might assist to interpret changes in diseased EIM measurements, and explain cross-sectional variations among healthy subjects; and (ii) increasing the excitation IED for a fixed sense IED, or reducing the sense IED for a fixed excitation IED, increases the contributions from muscle. However, the sensitivity analysis was performed on a non-anatomical geometry. Therefore, it leaves the impact of anatomical differences unanswered. The aforementioned FEA works have mainly focused on EIM for the assessment of neuromuscular disorders. Nonetheless, FEA has not been used to study EIM for the assessment of muscle activity until recently. This was brought up in [12], [13], where FEA was used to optimize EIM electrode configurations to monitor muscle fatigue. In [12], frequency and sensitivity studies over the 10KHz-100KHz range were performed on a cylindrical model of the upper arm, for two different electrode configurations. In [13], frequency study only at 50KHz was performed on an elliptical cylinder model of the upper arm. Current density ratio and sense potential were used to optimize the IED of a linear electrode array. These two works have demonstrated that the electrode arrangement affects the resistance change due to muscle contractions.

Previous works have significantly contributed to studying the biophysical mechanisms of EIM and improving the design of electrode arrangements. Nonetheless, to the authors' knowledge, none of them combines the aforementioned approaches over a wide frequency range as it might be required for an extensive and more detailed assessment of optimal recording frequencies and IEDs. Additionally, while these studies can be successfully used to develop clinical standards, they cannot be employed for developing EIM measurement systems. Further development of EIM technology and advanced measurement systems requires systematic design flows and circuit-based models that can be used in commercial circuit design environments. Circuit-based models offer advantages compared to finite element models, especially in terms of computational cost, and capability to study interactions with readout circuits, which might speed up the development of EIM measurement systems. To boost the development of EIM technology, we propose a circuit-based modelling methodology originated from FEA, which can be used to accurately emulate tissues and effects from parametric changes of subcutaneous fat and muscle thickness on EIM measurements. The proposed methodology studies EIM in terms of its biophysical mechanism through FEA over a wide frequency range, and complements the previous methodologies with circuit-based modelling. More specifically, combining the approaches from [9]–[12], FEA is used to evaluate bioimpedance spectrum (computed from the resulting Z-parameters), sensitivity distribution, and volume impedance density, for parametric changes of subcutaneous fat and muscle thickness on limb models, over the $1\,Hz-1\,MHz$ frequency range. Bioimpedance spectra shows the impact of alterations in subcutaneous fat thickness, muscle size, and IEDs on the EIM measurement. Impedance sensitivity and density is used to compute the contributions of tissues over the frequency range. From these contributions, the optimal recording frequency and IED is determined to maximize the muscle contributions. The lower end of the frequency range is extended from $1\,KHz$ to $1\,Hz$ to guarantee causality of the circuit model time response, when it is computed from its frequency response. Resulting FEA Z-parameters, on the limb models at each considered IED, are imported into a circuit design environment where a three Cole dispersion circuit-based model is developed for each set of Z-parameters. The methodology is demonstrated for particular cases of EIM on the upper arms and lower legs, and is validated by comparing FEA and circuit simulation results with EIM measurements on the respective limbs of ten human subjects.

The rest of the paper is organized as follows: Section II describes the methodology, including FEA, circuit modelling and simulations, and EIM measurements on human subjects. Section III explains and compares the results from the aforementioned studies. Section IV discusses the advantages and limitations of the proposed methodology. Section V concludes the work.

II. Methodology

A. Biophysical Principles Affecting EIM Measurements

Before explaining the proposed methodology, it is worth introducing the most important biophysical principles, which affect the EIM measurement and need to be modelled. The electrical behavior of biological tissue is defined by its dielectric properties, i.e. relative permittivity (ε_r) and conductivity
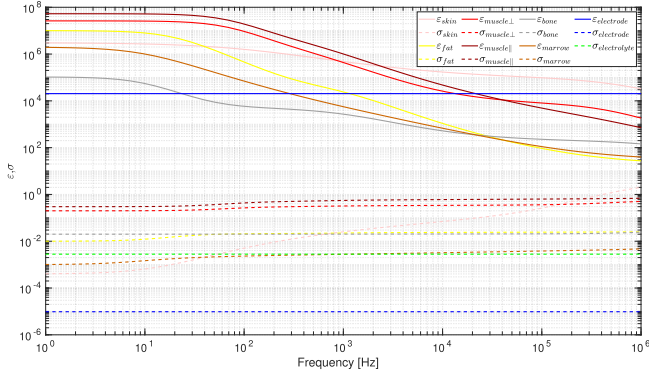
Fig. 1. Modelled dielectric properties of biological tissues, electrodes, and electrolyte.

(σ). These dielectric properties have a direct impact on the measured impedance. The modelled properties of biological tissue, electrodes, and electrolyte, are shown in Fig. 1. It can be seen that the dielectric properties of muscle are anisotropic. These properties are different depending on the direction of current flow in muscle fibers, i.e. in parallel or transverse. The expressions of the dielectric properties of tissues are based on 4-Cole-Cole dispersions, and are given by [8]:

$$\varepsilon_r = \varepsilon_\infty + \sum_{m=1}^{4} \frac{\Delta\varepsilon_m}{1 + (j\omega\tau_m)^{(1-\alpha_m)}} + \frac{\sigma_i}{j\omega\varepsilon_0} \quad (1)$$
$$\sigma = -\,\mathrm{Im}(\varepsilon_r)\omega\varepsilon_0$$

where ε_∞ is the relative permittivity at infinite frequency, $\Delta\varepsilon_m$, τ_m, and α_m represent the magnitude, time constant, and broadening of each dispersion region, σ_i is the ionic conductivity, ω is the angular frequency, and ε_0 is the permittivity of free space. The effects of dielectric properties on EIM measurement, considering a given geometry due to a limb's anatomy, can be quantitatively explained from a simplified expression of tissues' impedance [14]:

$$\begin{cases} Z = R \parallel \frac{1}{j\omega C} = \frac{R}{1 + j\omega RC} \\ R \propto \frac{1}{\sigma} \quad C \propto \varepsilon_r \end{cases} \quad (2)$$

where ε_r, and σ are the relative permittivity, and conductivity of the material/tissue, respectively. The impedance (Z), is the parallel combination of the resistive (R) and capacitive (C) components of tissue. In general, current flows through the path of lower impedance. When the IED increases, the injected current flows deeper into tissues, finding the paths of lower impedance through a larger conductive volume. When ω increases, the capacitance of each tissue acts as a path of low impedance, thus the magnitude of each tissue's Z decreases. When muscle volume relative to other tissues is much larger, most of the current will flow through muscle, in parallel with muscle fibers. Therefore, it can be expected that increasing the IED leads to larger muscle contributions to the measured impedance. However, given the frequency dependencies of ε_r and σ for each tissue, it is more difficult to predict *a priori* the optimal frequency at which the contributions from muscle are maximized for a particular limb. Therefore, simulations or

experimental measurements are required to estimate the optimal frequency. Nonetheless, a theoretical framework for predicting bioimpedance measurements of nonhomogeneous tissues has been recently proposed in [15], and could be used to theoretically estimate optimal IEDs and frequencies.

B. Finite Element Analysis

The FEA was performed using the AC/DC module, Electric Currents Physics from Comsol Multiphysics Software, version 5.3. The simplified geometrical models of an upper arm and lower leg were based on anatomical data from published sources [16]. Limb models consisted of skin, subcutaneous fat, muscle, cortical bone, and bone marrow, as well as surface electrodes with their respective electrolytes (see Fig. 2). The dielectric properties of biological tissues, i.e. relative permittivity (ε_r) and conductivity (σ), were taken from a reference database from published sources [5]–[8]. Tissues' parameters ($\varepsilon_\infty, \Delta\varepsilon_i, \tau_i, \alpha_i,$ and σ) were taken from "skin (wet)," "fat," "muscle (parallel fiber)," "muscle (transverse fiber)," "bone (cortical)" and "marrow (not infiltrated)" in the database. The skin dielectric parameters were adjusted from the reported values on [6], within the reported spreads, based on measurement data from one subject. Muscle's diagonal anisotropy was accounted by defining the relative permittivity and conductivity tensors of muscle ($\varepsilon_{r,m}, \sigma_{r,m}$) as:

$$\varepsilon_{r,m} = \begin{bmatrix} \varepsilon_{r,m\perp} & 0 & 0 \\ 0 & \varepsilon_{r,m\perp} & 0 \\ 0 & 0 & \varepsilon_{r,m\parallel} \end{bmatrix}$$

$$\sigma_{r,m} = \begin{bmatrix} \sigma_{r,m\perp} & 0 & 0 \\ 0 & \sigma_{r,m\perp} & 0 \\ 0 & 0 & \sigma_{r,m\parallel} \end{bmatrix} \quad (3)$$

where $\varepsilon_{r,m\parallel}, \varepsilon_{r,m\perp}, \sigma_{r,m\parallel}, \sigma_{r,m\perp}$ are the relative permittivity and conductivity, in parallel and transverse to the muscle fibers, respectively. Dielectric properties of the remaining body tissues were modelled as isotropic. Electrodes and electrolyte (electrode-tissue interface) dielectric properties were derived from previously published impedance models [17], and were also assumed isotropic. It is worth mentioning that the models in [8] are based on measurements from [7] with spreads of around 15-25% at frequencies below 100KHz, due to natural variability of structure and/or composition of biological tissues. Moreover, larger errors at frequencies below 1KHz might be present in these models due to electrode polarization. These uncertainties will consequently limit the accuracy and validity of the FEA. This will be discussed in further detail in Section IV.

The FEA consists of a frequency domain study over $1\,Hz - 1\,MHz$ range, with 10 linearly spaced points in the $1\,Hz - 976.53\,Hz$ sub-range, and 10 logarithmically spaced points in the $976.53\,Hz - 1\,MHz$ sub-range, for a total of 20 frequency points. Maxwell equations in quasi-electrostatic field condition were used to model the EIM measurement in this
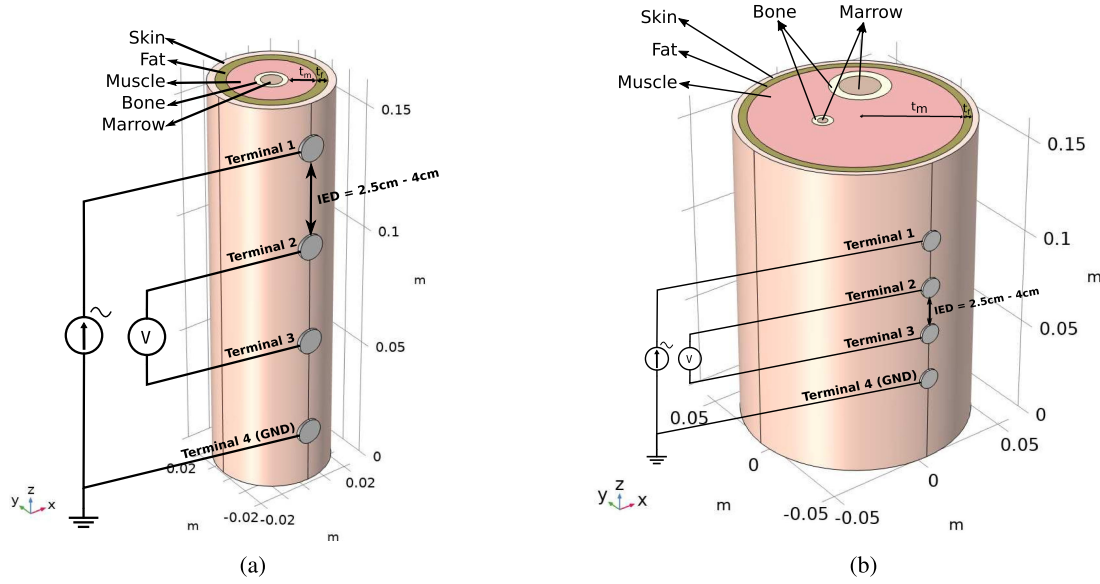
Fig. 2. FEA geometrical models of the upper arm (a) and lower leg (b). Terminal 1 represents the electrode connected to the current source, Terminals 2 and 3 represent the electrodes with floating potentials. Terminal 4 represents the electrode connected to the current sink (ground reference or GND). (a) Upper Arm. (b) Lower Leg.

frequency range, as follows:

$$
\begin{cases}
\nabla \cdot \vec{J} = \vec{Q_j} \\
\vec{J} = (\sigma + j\omega\varepsilon_0\varepsilon_r)\vec{E} + \vec{J_e} \\
\vec{E} = -\nabla \cdot V
\end{cases}
\tag{4}
$$

where $\vec{J}\,(A/m^2)$ is the current density, $\vec{Q_j}\,(A/m^3)$ is the distributed current source, $\vec{E}\,(V/m)$ is the electric field, $\vec{J_e}\,(A/m^2)$ is the external current density, and $V\,(V)$ is the electric potential.

Boundary conditions were set to ensure continuity of the current density and electric potential between contiguous tissue layers, electrode-tissue interfaces, and electrodes. Electrodes' surfaces were set as terminals. More specifically, the outer electrodes were set as current source and sink (ground) respectively, while the inner electrodes were set as floating potentials (no current flow into the electrodes), thus allowing to measure the voltage under them. The injected current was set to $10\,\mu A$ in accordance to the measurement equipment. The outer boundary surfaces of the remaining geometry were set as electrically insulated. The models of an upper arm and lower leg, including electrodes and associated interfaces, are shown in Fig. 2. The mesh was automatically generated in Comsol, using these models' physics (physics-controlled mesh). The mesh resulted in 103 855 and 277 699 tetrahedral elements for the upper arm and lower leg models, respectively.

During FEA, two parametric sweeps over the aforementioned models were performed. In the first sweep, geometrical parameters such as IEDs, subcutaneous fat thickness (t_f), and muscle thickness (t_m) were swept. The analyzed IEDs were $2.5\,cm$ and $4\,cm$, assuming equally spaced electrodes. Subcutaneous fat thicknesses were taken in 5 linear steps from $4\,mm$ to $12\,mm$. Muscle thicknesses were taken in 5 linear steps from $8\,mm$ to $16\,mm$ for the upper arm, and $50\,mm$ to $58\,mm$ for the lower

leg. In the second parametric sweep, which is a manual terminal sweep, Z-parameters were generated in order to compute the terminals impedance. The resulted Z-parameters were exported into a touchstone file for later use in a circuit design environment. The FEA was computed with Comsol's MUMPS direct solver, using 8 threads from an Intel Core i7-4770 CPU at 3.4 GHz.

1) Bioimpedance Spectroscopy: The bioimpedance spectrum was calculated from the resulted Z-parameters. Given that the EIM measurement can be modelled as a 3-port network with a ground reference (terminal 4), the frequency dependent Z-parameters are given by:

$$
Z(f) = \begin{bmatrix}
Z_{11} & Z_{12} & Z_{13} \\
Z_{21} & Z_{22} & Z_{23} \\
Z_{31} & Z_{32} & Z_{33}
\end{bmatrix}
\tag{5}
$$

where sub-indexes stand for the terminal number, with terminal 1 being the current source, and terminals 2 and 3 being the floating potentials, as in Fig. 2. Considering that we are only interested in the impedance given by the voltage difference between the inner electrodes over the injected current, the impedance spectrum can be computed as:

$$
Z_{EIM}(f) = Z_{21} - Z_{31}
\tag{6}
$$

from where magnitude and phase are calculated as:

$$
|Z_{EIM}| = \sqrt{\mathrm{Re}(Z_{EIM})^2 + \mathrm{Im}(Z_{EIM})^2}
$$

$$
\angle Z_{EIM} = \arctan\left[\frac{\mathrm{Im}(Z_{EIM})}{\mathrm{Re}(Z_{EIM})}\right]
\tag{7}
$$

2) Impedance Sensitivity and Density Studies: The total measured bioimpedance is the result of multiple tissues' contributions. Therefore, it is useful to find the impedance sensitivity

for each constituent tissue so that each contribution can be quantified and analyzed independently [11]. Impedance sensitivity is defined as:

$$S = \frac{\vec{J_1} \cdot \vec{J_2}}{I_s^2} \qquad (8)$$

where I_s is the amplitude of the applied current, and $\vec{J_1}$ (A/m^2) and $\vec{J_2}$ (A/m^2) are current densities when current source and sink (ground) are set on the outer electrodes and the inner electrodes, respectively. Impedance density is calculated as [18]:

$$Z_v = \frac{\left\| \vec{E_1} \right\|}{\left\| \vec{J_1} \right\|} \cdot S \qquad (9)$$

where $\vec{E_1}(V/m)$ is the electric field when current source and sink are set on the outer electrodes. Then, the impedance contribution from each tissue and the total impedance can be calculated as [18]:

$$\begin{cases} Z_i = \int_{V_i} Z_v \, dv \\ Z_{total} = \sum_{i=1}^{5} Z_i \end{cases} \qquad (10)$$

where $i = [1, 5]$ and it represents the tissue sub-domain, i.e. skin, fat, muscle, bone, and marrow. Given that the impedance contribution from each tissue can be represented as a vector in a complex plane, it is possible to calculate the contribution to the total impedance from the scalar projection ($comp_{Z_i} Z_{total}$) as:

$$cont_i = \frac{comp_{Z_i} Z_{total}}{\sum_{i=1}^{5} comp_{Z_i} Z_{total}} = \frac{\mathrm{Re}(Z_i \cdot \overline{Z_{total}})}{\sum_{i=1}^{5} \mathrm{Re}(Z_i \cdot \overline{Z_{total}})} \qquad (11)$$

In Eq. (8), it can be seen that depending on the relative orientation of complex current density vectors ($\vec{J_1}$ and $\vec{J_2}$) to each other, the real and imaginary values of sensitivity (S) can be positive, negative, or zero. Moreover, the impedance density (Z_v) is proportional to S, as can be seen in Eq. (9). Therefore, the impedance contribution from a single tissue (Z_i), resulting from the sum of S in every infinitely small region within its respective volume, as seen in Eq. (10), can result in a complex value with any direction in the complex plane. Regions with zero sensitivity, will not add to Z_i. On the contrary, regions with positive or negative sensitivity will define the direction and magnitude of Z_i. The possibility of Z_i pointing in the opposite direction of the total impedance (Z_{total}) might result in an individual tissue contribution that is negative or positive exceeding Z_{total}. Nonetheless, the cumulative impedance from every tissue, Z_i, always results in Z_{total}. Consequently, since the contribution from each tissue is the scalar projection of Z_i over Z_{total}, normalized to the sum of scalar projections from every tissue, as seen in Eq. (11), the sum of all contributions must add to a total of 1, which is 100% of Z_{total}. In essence, this definition of the contribution shows how much each Z_i vector points in the direction of Z_{total}. Negative percentage contributions mean that the projection of Z_i on Z_{total} is pointing in the opposite direction
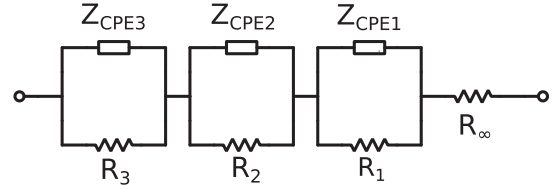

Fig. 3. Circuit model of the limbs' bioimpedance based on three Cole dispersions.

in the complex plane, while positive percentage contributions mean that the projection points in the same direction.

C. Circuit Modelling and Simulations

Circuit simulations were performed with Spectre Circuit Simulator from Cadence Virtuoso Analog Design Environment, using 8 threads from an Intel Xeon ES-2630v3 CPU at 2.46GHz. The processing capability of this CPU is comparable to the one were FEA was performed. The resulting Z-parameters from FEA were imported into the circuit simulation environment. More specifically, a linear 3-port network block with a ground reference was used to simulate the EIM measurement, taking its characteristics from the Z-parameters' touchstone file. Both AC and time domain simulations were performed to develop and validate the model. Spline interpolation and extrapolation of the frequency domain data were used to calculate the impulse response to allow for convolution-based solving methods in time domain simulations.

1) Circuit Model of Limbs' Bioimpedance: A simple circuit model based on three Cole dispersions, shown in Fig. 3, was extracted to model the resulting bioimpedance from the EIM measurement. Each dispersion region is modelled as the parallel combination of a resistor R_i, and a constant phase element (fractional pole) $Z_{CPEi} = 1/C_i(j\omega)^{\alpha_i}$ [19], where $i = [1, 3]$ represents the dispersion region's number. The frequency ranges of each dispersion region: $1 \, Hz - 1 \, KHz$, $1 \, KHz - 100 \, KHz$, and $100 \, KHz - 1 \, MHz$, were determined from a visual inspection of the FEA bioimpedance spectrum. The model's impedance is given by:

$$Z_{cm} = R_\infty + \sum_{i=1}^{3} \frac{R_i}{1 + R_i C_i (j\omega)^{\alpha_i}} \qquad (12)$$

where R_∞ represents the parallel combination of the resistance caused by intracellular and extracellular mediums, at infinite frequency [1].

2) Model Fitting Methodology: The circuit model parameters, i.e. R_∞, R_i, C_i, and α_i, were obtained by minimizing the error between its AC response and that of the 3-port network described by Z-parameters. Each parameter was obtained by minimizing the impedance magnitude error in different frequency regions, using the Levenberg-Marquardt algorithm. Magnitude was chosen for the model fitting since it resulted in a better match than fitting phase, resistance, reactance, or overall impedance expression, given that the model parameters are bound to real values. More specifically, R_∞ was obtained by fitting data at the maximum simulated frequency ($1 \, MHz$), while R_i, C_i, and

α_i were obtained by fitting data at their respective dispersion regions.

Once the first set of model parameters were found for the nominal fat and muscle thickness, the process was repeated for increased thickness of the aforementioned tissues, in order to observe their respective dependencies. For simplicity, it was assumed that R_∞ and α_i were constant, given that their dependencies with fat and muscle thickness were negligible, as observed through the model fitting process.

D. Electrical Impedance Myography Measurements on Human Subjects

Measurements on ten healthy human subjects (4 male and 6 female, 20 to 30 years old) were performed. The measurements were compared with the FEA and circuit simulation results, to evaluate the methodology's accuracy. The positions of biceps brachii and gastrocnemius muscles were identified before skin preparation and placement of electrodes on subjects. Skin preparation was done in order to improve electrode adhesion and lower the skin impedance by removing oils, sweat, and stratum corneum. Skin preparation consisted of shaving the area (if needed), followed by mild skin abrasion with a fine sandpaper (120 grit), disinfection of the area with an alcohol based solution, and drying with cotton. Electrodes (3 M red-dot-2228) were then placed in the middle of the biceps brachii muscle and the medial head of the gastrocnemius muscle in a linear array with IEDs of $2.5\,cm$ and $4\,cm$. Electrodes were replaced after each measurement, thus reducing contact artifacts in the data.

Measurements were carried out with a custom-made hardware, based on an updated version of the bioimpedance sensor developed in [20] (calibration data is provided in this reference under Section IV. A, B). This hardware was connected to a computer over Bluetooth and the bioimpedance spectrum data was read-out with a custom-made software. Measurements were performed on subject limbs while keeping their muscles relaxed. More specifically, the subjects were asked to keep their arms extended and their lower legs suspended on a neutral position. Each measurement consisted of 10 samples of the bioimpedance spectrum from which the average value and root mean square (RMS) errors were extracted. The measurement was repeated 5 times for each limb, resulting in a total of 20 measurements, i.e. 10 measurements on the upper arms and 10 measurements on the lower legs. Each measurement sample consisted of 10 logarithmically spaced points in the $976.53\,Hz - 1\,MHz$ range. Combined average values and RMS errors were extracted from all measurements on each pair of limbs.

KTH Royal Institute of Technology's ethical advisor reviewed the details of this experiment and concluded that it did not require ethical permission from the Swedish Ethical Review Board.

III. RESULTS

A. FEA and Circuit Modelling

1) Individual Tissues' Contributions to the Total Bioimpedance: Individual tissues' contributions to the total impedance of the upper arm and lower leg, for IEDs of $2.5\,cm$

and $4\,cm$ are shown in Fig. 4. For a given IED, the sum of all individual tissues' contributions is 100%, at each frequency. Details on the expression and meaning of the contributions have been provided in Section II.B.2. Although impedance sensitivity, volume impedance density, and individual tissues' contributions were calculated for the entire frequency range of study ($1\,Hz - 1\,MHz$), only the $15.625\,KHz - 250\,KHz$ range is shown to facilitate the analysis, given that in this range muscle contributions are maximized as compared to the rest of tissues. The results over the whole studied frequency range can be seen in [21].

An ideal EIM measurement maximizes the muscle contribution while minimizing contributions from the rest of tissues, i.e. as close to zero as possible. This is achieved at around $31.25\,KHz$ for the upper arm and at around $62.5\,KHz$ for the lower leg, as it can be seen in Fig. 4. These results are consistent with previous studies [22], [23], where experimental data shows that the EIM measurement is more reactive to changes in muscle around these frequencies. Therefore, this confirms that there is good matching between theory and measurement data. Nonetheless, these results also show that the optimal frequency for EIM measurements varies for different limbs. Moreover, it can be observed that muscle contributions as compared to the rest of tissue is larger for an IED of $4\,cm$ than for $2.5\,cm$, for both models. This can be explained using Fig. 5, where a larger area of positive sensitivity (normalized to the maximum sensitivity) can be seen at the muscle tissue layer in Fig. 5(b) and Fig. 5(d) as compared to Fig. 5(a) and Fig. 5(c). The positive and negative sensitivity regions in the skin layer cancel out skin contributions at the optimal frequency. In a similar manner, the positive and negative sensitivity regions in the subcutaneous fat layer reduces contributions from fat at $4\,cm$ IED as compared to $2.5\,cm$ IED, where mostly positive sensitivity regions are observed.

2) Bioimpedance Spectrum From FEA and Circuit Model: Given that muscle contributions are generally larger for an IED of $4\,cm$ than for $2.5\,cm$, only the results for $4\,cm$ will be shown. Nonetheless, the results for $2.5\,cm$ can be seen in [21].

The bioimpedance spectrum results from FEA of the upper arm model and its corresponding circuit model are shown in Fig. 6. The dependencies with subcutaneous fat and muscle thickness (t_f and t_m, respectively) can be evaluated in terms of the root-mean square rate of change (RMSROC) over their respective range of variation, as obtained from FEA. As it can be seen in Fig. 6(a), magnitude increases as t_f increases in the $1\,Hz - 10\,KHz$ range, while magnitude slightly decreases with increasing t_f in the $10\,KHz - 1\,MHz$ range. The magnitude's RMSROC with respect to t_f is $3.98\Omega/mm$. Moreover, it can be seen that the circuit model magnitude matches that of FEA with negligible deviations over the entire frequency range. Unfortunately, as it can be seen in Fig. 6(b), matching is not as accurate for the phase. However, phase responses follow the same trend. It can be seen that as t_f increases, the low and high frequency peaks of the phase response shift towards lower frequencies, with an RMSROC of $0.32°/mm$. Fig. 6(c) shows that over the entire frequency range, magnitude increases as t_m increases, with a RMSROC of $3.04\Omega/mm$. It can be seen also that for magnitude's variation with t_m, there is also good
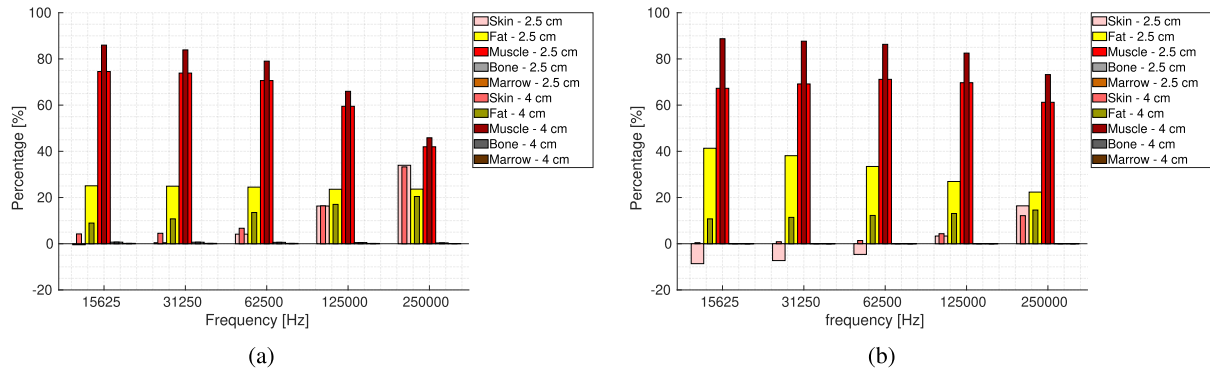
Fig. 4.   FEA Impedance Sensitivity and Density Study - Percentage contributions of tissues to bioimpedance. (a) Upper Arm. (b) Lower Leg.
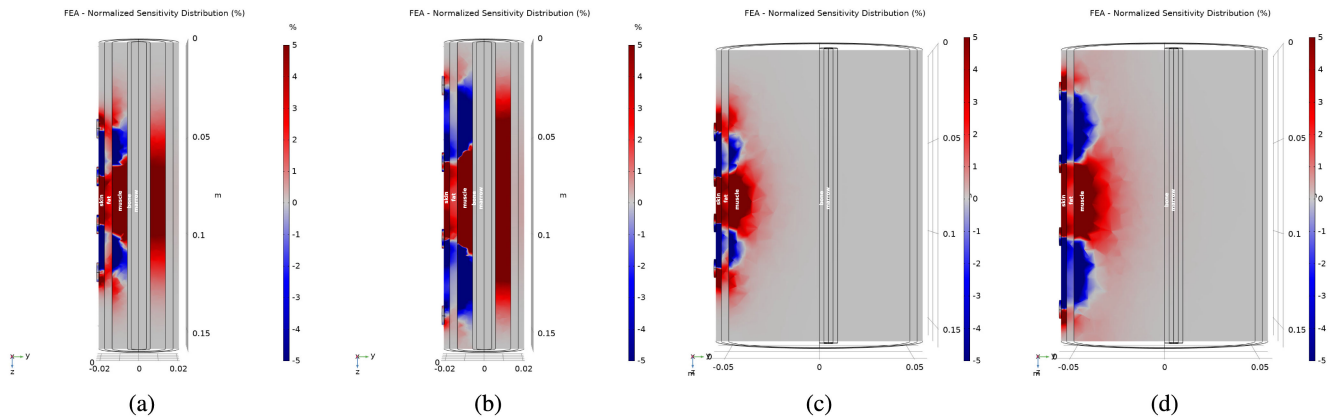

Fig. 5.   Normalized sensitivity distribution on longitudinal cross-section of the upper arm (a), (b) and lower leg (c), (d) models at $62.5\,KHz$ and $125\,KHz$, respectively. Grey opaque lines represent the tissues' geometrical boundaries. The blue-red color scale represent normalized sensitivity values. (a) Upper Arm - $2.5\,cm$ IED. (b) Upper Arm - $4\,cm$ IED. (c) Lower Leg - $2.5\,cm$ IED. (d) Lower Leg - $4\,cm$ IED.

matching between circuit model and FEA. The phase responses of the circuit model and FEA follow the same trend, despite discrepancies in their values (Fig. 6(d)). It is clear that the high frequency peak increases as t_m increases. This happens with a RMSROC of $0.14°/mm$.

The bioimpedance spectrum results for the lower leg model are presented in Fig. 7. The behavior of bioimpedance spectra with respect to t_f and t_m is similar to that of the upper arm. Fig. 7(a) and Fig. 6(b) show good magnitude matching, deviations in the phase, and same trends between circuit model and FEA. The magnitude's and phase's RMSROCs with respect to t_f are $3.69\Omega/mm$ and $0.10°/mm$, respectively. There are also less significant differences in the magnitude and phase responses with t_m as compared to the upper arm (see Fig. 7(c), 7(d)). This is evident from the RMSROC values of magnitude and phase, which are $0.41\Omega/mm$ and $0.01°/mm$, respectively.

3) Dependencies of Circuit Model Parameters With Fat and Muscle Thickness: Dependencies of the circuit model parameters (R_i and C_i) of the upper arm and lower leg with t_f and t_m are shown in Fig. 8. The circuit parameters dependencies provide an intuitive understanding of bioimpedance spectrum changes due to anthropometric variations. For the upper arm and lower leg models, resistance associated with each dispersion region (R_{1-3}) increases with t_f (Fig. 8(a) and Fig. 8(c)).

These changes in resistances explain the overall increase of magnitude. It can be seen that the capacitance associated with each dispersion region (C_{1-3}) changes less significantly with t_f as compared to the resistance in each respective region. These small changes in capacitance in conjunction with the more significant increase in resistance moves the poles of the impedance towards lower frequencies (see Eq. (12)). This causes the shift of low and high frequency phase peaks towards lower frequencies. Contrary to the case of increasing t_f, resistance associated with each dispersion region (R_{1-3}) decreases with increasing t_m (Fig. 8(b) and Fig. 8(d)). Note that this is the case for all parameters, except for R_2 which increases slightly. This also explains the overall decrease of magnitude, although less pronounced in Fig. 8(d) as compared to Fig. 8(b). For the upper arm model, capacitance associated with each dispersion region (C_{1-3}) increases as t_m increases, while for the lower leg model these capacitances remain practically constant. In this case, the increase in capacitance compensates for the reduction in resistance, thus keeping the poles in the same position, while increasing the phase peak (Q-factor). For the lower leg model, the small changes in resistance and capacitance do not cause any significant change in the bioimpedance spectrum.

4) Quantitative Comparison of FEA and Circuit Model: Impedance spectra of the circuit-based model and FEA was
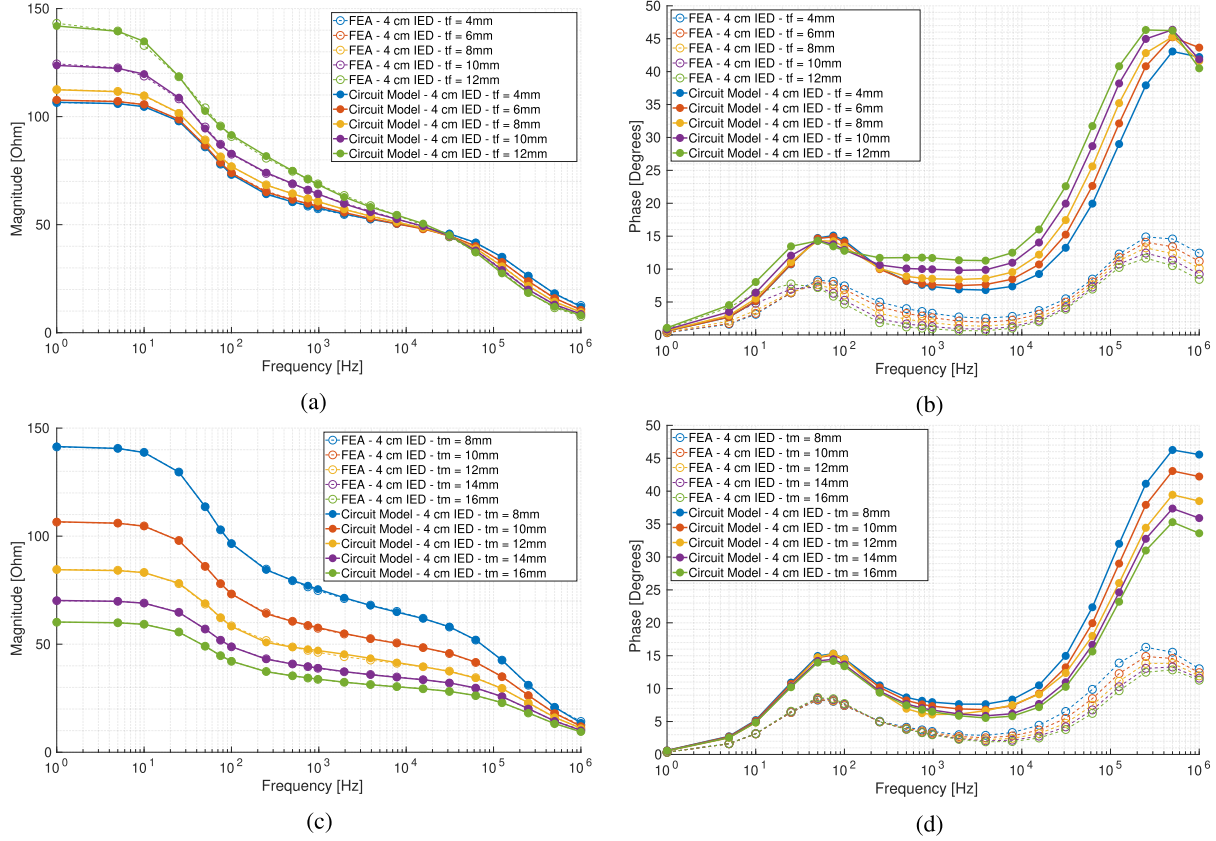
Fig. 6. Resulting impedance spectrum from FEA and circuit model of the upper arm for an IED of 4 cm. Influence of fat and muscle thickness on the spectrum is shown in (a)-(b), and (c)-(d), respectively. (a) Magnitude - Change in Fat Thickness. (b) Phase - Change in Fat Thickness. (c) Magnitude - Change in Muscle Thickness. (b) Phase - Change in Muscle Thickness.

TABLE I
RMSE AND RMSEROC WITH RESPECT TO t_f AND t_m FOR THE UPPER ARM AND LOWER LEGS FOR AN IED OF $4\ cm$

	Upper Arm		Lower Leg	
	Magnitude	Phase	Magnitude	Phase
RMSE - t_f	0.42Ω	15.08°	0.22Ω	11.60°
RMSE - t_m	0.27Ω	11.17°	0.06Ω	5.79°
RMSEROC - t_f	$0.13\frac{\Omega}{\text{mm}}$	$0.90\frac{\circ}{\text{mm}}$	$0.05\frac{\Omega}{\text{mm}}$	$1.30\frac{\circ}{\text{mm}}$
RMSEROC - t_m	$0.07\frac{\Omega}{\text{mm}}$	$0.46\frac{\circ}{\text{mm}}$	$0.005\frac{\Omega}{\text{mm}}$	$0.04\frac{\circ}{\text{mm}}$

compared using the combined root-mean square error (RMSE) for every t_f and t_m. Likewise, the spectra dependencies with t_f and t_m was compared using the root-mean square error of the rate of change (RMSEROC). The RMSE and RMSEROC with respect to t_f and t_m can be seen in Table I. The low values of magnitude RMSE and RMSEROC demonstrate that high accuracy can be obtained for magnitude responses of the proposed circuit model. The considerably lower accuracy of the phase response as compared to the magnitude is clear from the relatively large values of phase RMSE. However, the relatively low values of RMSEROC demonstrate that the accuracy in the trends for variations of t_f and t_m is much higher. It can also be noticed that the accuracy of the magnitude and phase responses is higher for variations of t_m than for variations of t_f.

FEA and circuit-based model simulations were also compared in terms of their computation times obtained from the corresponding simulation environments. Single solution computation time of FEA was obtained from dividing the total simulation time by the number of parameter combinations (100). Total simulation time of the upper arm model was $45\ min$ $34\ s$, thus $27.34\ s$ per solution. For the lower leg model, the computation time was $2\ h\ 6\ min\ 41\ s$, thus $76.01\ s$ per solution. The circuit model computation time for a single set of parameters was $0.853\ s$, and it was approximately the same for each set of parameters. Therefore, the circuit model can be computed 32 times faster than FEA for the upper arm model, and 89 times faster for the lower leg model, using equivalent processing power.

B. Comparison of Models and EIM Measurements on Human Subjects

The comparison of bioimpedance spectrum from FEA, circuit model, and EIM measurements on subjects' upper arms and lower legs is presented in Fig. 9. Measurement data from ten subjects at $2.5\ cm$ and $4\ cm$ IED is represented in two grouped box plots. For the upper arms, fat and muscle thickness of $4\ mm$ and $10\ mm$, respectively have been considered in the models, while for the lower leg, fat and muscle thickness of $6\ mm$ and $50\ mm$ have been considered. As earlier, RMSE was used to compare the accuracy of FEA and circuit model to the average value from human subjects measurements, as seen in Table II.
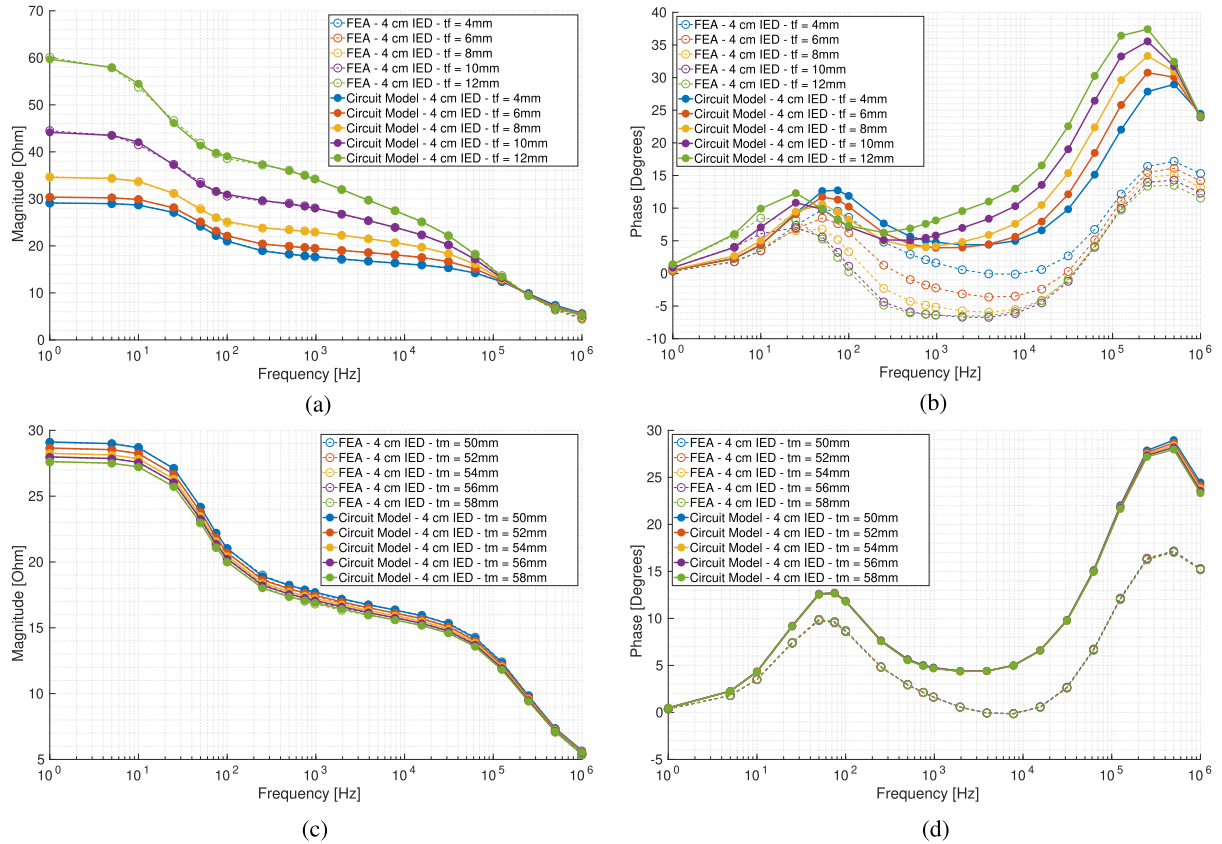
Fig. 7.   Resulting impedance spectrum from FEA and circuit model of the lower leg for an IED of 4 cm. The influence of fat and muscle thickness on the spectrum is shown in figures (a)-(b) and (c)-(d), respectively. (a) Magnitude - Change in Fat Thickness. (b) Phase - Change in Fat Thickness. (c) Magnitude - Change in Muscle Thickness. (d) Phase - Change in Muscle Thickness.

TABLE II
FEA AND CIRCUIT MODEL RMSE FOR THE UPPER ARM AND LOWER LEGS

	Upper Arm		Lower Leg	
	Magnitude	Phase	Magnitude	Phase
RMSE - 4cm - FEA	29.59Ω	4.32°	19.59Ω	3.62°
RMSE - 2.5cm - FEA	36.59Ω	4.36°	26.97Ω	3.44°
RMSE - 4cm - circuit	29.59Ω	7.60°	19.58Ω	8.97°
RMSE - 2.5cm - circuit	36.43Ω	15.05°	26.83Ω	17.28°

Fig. 9(a) and Fig. 9(c) show that the magnitude from FEA and circuit model have deviations from the mean values and spreads of measurements, which is clearly shown also by the relatively large magnitude RMSE values. However, the models' magnitude follows a similar trend as the measured data. Fig. 9(b) and Fig. 9(d) show that the phase response from FEA matches measurements on subjects quite accurately, which is also confirmed by the low phase RMSE value of FEA at both IEDs. Nonetheless, as it can be expected from the previous subsection results, phase values of the circuit model deviate from measurements, and phase RMSE values are large, although the phase responses follow the same trend. Additionally, the box plots spreads show that the measured impedance spectra (magnitude and phase) differ between subjects. Moreover, the measured minimum and maximum values (whiskers) are considerably further away from the spreads in magnitude as compared to phase. It is worth mentioning that a few outliers are found over the frequency

range, with generally larger deviations from the mean at the lower end of the spectrum. Additionally, the circuit model and FEA bioimpedance spectrum is generally more accurate for an IED of $4\,cm$ than $2.5\,cm$.

IV. DISCUSSION

In this work, we proposed a methodology with the aim of studying EIM in terms of its biophysical mechanism through FEA, and developing a simple circuit-based model which accurately emulates the tissues and effects of parametric changes of subcutaneous fat and muscle thickness. The key findings can be summarized as follows:

(i) There is an optimal frequency for which the muscle contribution is maximized while the contributions of other tissues is minimized. It was found that the optimal frequency is different for each of the studied limbs. This is supposed to be mainly caused by relative muscle volume with respect to the other tissues as this is the main parametric difference between the upper arm and lower leg models, considering that contributions from bone and marrow are negligible (see Fig. 5), and skin thickness does not change considerably [24]. Anisotropic properties of muscle might also play a role in the optimal frequency. At around 50 KHz, the transverse permittivity of muscle is almost equal to the parallel permittivity, and thus the reactance is maximized. This essentially means that the impedance sensitivity and density
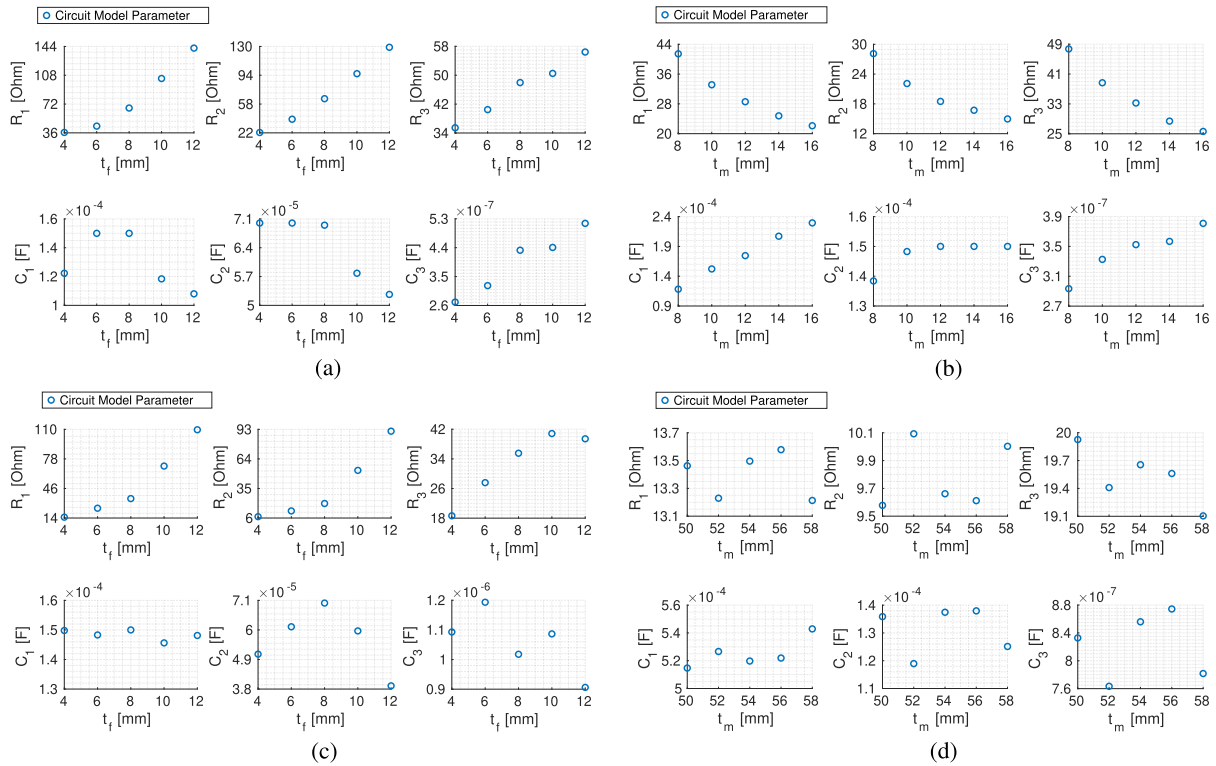
Fig. 8.   Dependencies of circuit model parameters of the upper arm and lower leg with fat and muscle thickness. (a) Upper Arm - Dependence with Fat Thickness. (b) Upper Arm - Dependence with Muscle Thickness. (c) Lower Leg - Dependence with Fat Thickness. (d) Lower Leg - Dependence with Muscle Thickness.
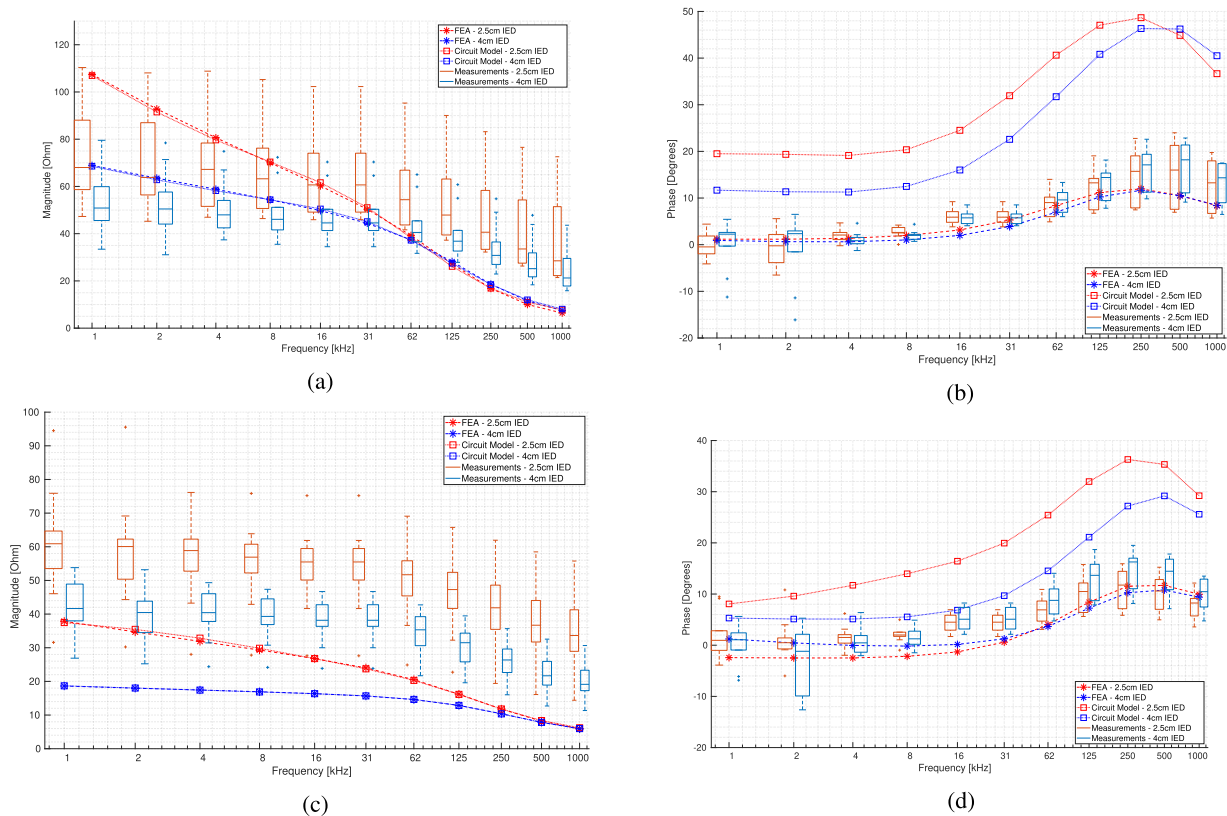

Fig. 9.   Comparison of bioimpedance spectrum from FEA, circuit model, and EIM measurements of subjects' upper arms and lower legs. (a) Magnitude - Upper Arm. (b) Phase - Upper Arm. (c) Magnitude - Lower Leg. (d) Phase - Lower Leg.

study might be a useful tool to evaluate the optimal frequency at which measurements should be carried on a given muscle. This is in addition to optimizing the electrode configuration, as it has been previously done in [10], [11].

(ii) Increasing distance between current injection electrodes (and in general, increasing distance between every electrode) increases the contributions of muscle, while reducing subcutaneous fat contributions to the measured impedance of both limbs. This finding is consistent with previous studies [10], [11] where parametric variations of the geometries and sensitivity analysis were used to optimize the electrode configurations. This might be partially caused by the anisotropy of muscle's dielectric properties. As the excitation IED increases, current flows through larger volumes, and large permittivity and conductivity in parallel to the muscle fibers in comparison to other tissues results in more current flowing through muscle, and thus an increase of its contributions. Given that the effect of electrode placement was similar on both limbs, these findings could be generalized for measurements on any muscle. However, it might be necessary to do studies with more detailed models that account for other types of tissues, which might have a stronger effect on regions of the body with lower muscle volume relative to them.

(iii) The measured bioimpedance spectrum can be modelled with fair accuracy by a simple electrical circuit, based on three Cole dispersions. However, the phase response accuracy of the circuit model is limited. This phase inaccuracy is caused by circuit parameters being bound to real values. The capacitance that results from Eq. (2),(1), is a complex value, which is not supported by circuit simulators. This also implies that fitting the circuit model to other components of the impedance, i.e. real, imaginary, or phase, will not result in a significantly better fit. Nonetheless, the overall dependencies with subcutaneous fat and muscle thickness are preserved. Furthermore, the circuit model parameters have clear dependencies with subcutaneous fat and muscle thickness. These dependencies intuitively explain effects on bioimpedance spectra due to anthropometric variations. The proposed circuit-based model can be reliably used to emulate the EIM measurement in circuit simulations, and can be adjusted to individual subject's measurements or anthropometric data. Moreover, due to its simplicity, the circuit model can be quickly included in electronic circuit design environments, thus having an advantage over the FEA and 3-port network counterparts. Additionally, the circuit model has a significant advantage in terms of computation time as compared to FEA, as shown in Section III.A.4. This advantage could be even more significant as the complexity of geometries in FEA increases. Therefore, the circuit model allows time-efficient simulations at an early stage of EIM systems design. This would speed-up the design process and enable further design optimizations.

(iv) The FEA and circuit model results match the EIM measurement with different levels of accuracy. There are also clear differences between subjects' measured impedance spectra. This is expected mainly due to variations in subcutaneous fat thickness and muscle mass between subjects. These variations might also explain the longer whiskers in the magnitude as compared to the phase, given the magnitude's RMSROC. Nonetheless,

subject variability could also be partially caused by spreads in the dielectric properties of tissues, as noted in Section II.A. The outliers that are found over the frequency range could have been caused by artifacts in the measurement due to poor electrode contact. It is believed that the models' accuracy is limited by the simplicity of the FEA geometries, spreads in the modelled dielectric properties, and other physical effects that were not included in the FEA. For instance, these models did not include connective tissue, which is expected to have similar dielectric properties to those of subcutaneous fat [5]–[8]. Given that fat contributions to the total measurement increase with decreasing IED, it can be expected that connective tissue contributions will also increase. Moreover, inter-electrode capacitances were not included in the models. These are expected to have a larger effect on the measured impedance as the IED becomes shorter. Therefore, it can be generally expected that the models will have lower accuracy with decreasing IED, as identified in Section III.B.

The proposed methodology has also other limitations in terms of applicability on human subjects, which can be addressed by follow-up studies. As noted in Section II.A, the models of dielectric properties used in FEA are based on measurements with reported spreads. Consequently, it can be expected that the accuracy of the optimal frequency and IED, for which the muscle contributions are maximized on a specific subject, is limited. Nonetheless, since the simulated impedance follows a similar trend to the measured data, the proposed methodology can be used for approximating the optimal frequency and IED for a subject's limb, and potentially for other muscles in the human body. It is worth noting that sensitivity analysis also has certain limitations. As can be observed in Fig. 5, there are severely sharp boundaries between the positive and negative regions of sensitivity. This is due to current density vectors $\vec{J_1}$ and $\vec{J_2}$ being perpendicular to each other in these boundaries. As a result, the accuracy of individual and total impedance from tissues, calculated from sensitivity distribution, will be limited. Nonetheless, the contributions should not be affected by this inaccuracy, given that these result from normalized scalar projections. Therefore, sensitivity analysis remains as a useful tool to evaluate individual tissues contributions and optimal recording frequencies.

This study and the proposed methodology can be extended to provide additional value. Variability in subjects' anatomy can be accounted by using subject specific anthropometric data. Variability in the dielectric properties of tissues can be accounted through Monte-Carlo simulations. Using more detailed anatomical data to generate the FEA models could provide more accurate assessments. For instance, magnetic resonance imaging (MRI) data of the limb or muscle group of interest could potentially be used to generate the FEA's geometry and mesh, while providing higher level of detail for the constituent tissues through appropriate segmentation. Additionally, other electrode configurations could be explored and compared to the traditional linear array in smaller muscles, where the measurement area is more limited. Furthermore, if phase response with higher accuracy is required during circuit simulations, the resulting Z-parameters from FEA could be directly used in the circuit simulation environment at the cost of longer simulation times and possible convergence problems during DC operating point computations.

V. CONCLUSION

We presented a FEA and circuit modelling methodology to study EIM on upper arms and lower legs. The contributions of the modelled tissues to the total impedance were obtained through an impedance sensitivity and density study. The effects of the measurement frequency and IED on the aforementioned contributions were analyzed, and potentially optimal conditions under which the muscle contributions are maximized, were presented. It was found that muscle contributions are maximized at around 31.25 kHz and 62.5 kHz for the upper arm and lower leg, respectively, at 4 cm IED. The resulting Z-parameters from FEA were imported into a circuit design environment and used to extract the three Cole dispersions circuit-based model. The circuit model parameters were obtained by fitting the magnitude responses of the circuit model to those of the FEA for variations in subcutaneous fat and muscle thickness. The resulting fits show that the circuit model accurately represents the magnitude and phase responses of the FEA, despite deviations in the phase. The circuit model emulates variations in subcutaneous fat and muscle thickness, and simulates up to 89 times faster than FEA with equivalent processing power. These variations are represented by clear dependencies in the circuit model parameters. These dependencies provide an intuitive mean to understand and simulate the effects of anthropometric variations on the EIM measurement. FEA and circuit-level simulation results were compared with measurements on ten human subjects, showing fair agreement. The circuit model matches subjects measurements with RMS errors lower than 36.43Ω for the magnitude and $17.28°$ for the phase, while FEA does with errors lower than 36.59Ω and $4.36°$. Overall, the proposed methodology has the ability to accurately model the limbs bioimpedance and help EIM system designers to efficiently explore various design options.

REFERENCES

[1] B. Sanchez and S. B. Rutkove, "Electrical impedance myography and its applications in neuromuscular disorders," *Neurotherapeutics*, vol. 14, no. 1, pp. 107–118, 2017.

[2] B. Sanchez and S. B. Rutkove, "Present uses, future applications, and technical underpinnings of electrical impedance myography," *Curr. Neurol. Neurosci. Rep.*, vol. 17, no. 11, pp. 11687–11696, Dec. 2019.

[3] R. Kusche and M. Ryschka, "Combining bioimpedance and EMG measurements for reliable muscle contraction detection," *IEEE Sens. J.*, vol. 19, no. 23, pp. 11687–11696, Dec.2019.

[4] R. usche and M. Ryschka, "Multi-frequency impedance myography: The PhaseX effect," *IEEE Sens. J.*, vol. 21, no. 3, pp. 3791–3798, Feb. 2021.

[5] N. Carrara, "The dielectric properties of body tissues," 2020. [Online]. Available: http://niremf.ifac.cnr.it/tissprop/refs

[6] C. Gabriel, S. Gabriel, and E. Corthout, "The dielectric properties of biological tissues: I. literature survey," *Phys. Med. Biol.*, vol. 41, no. 11, pp. 2231–2249, 1996.

[7] S. Gabriel, R. W. Lau, and C. Gabriel, "The dielectric properties of biological tissues: II. measurements in the frequency range 10 hz to 20 GHz," *Phys. Med. Biol.*, vol. 41, no. 11, pp. 2251–2269, 1996.

[8] S. Gabriel, R. W. Lau, and C. Gabriel, "The dielectric properties of biological tissues: III. parametric models for the dielectric spectrum of tissues," *Phys. Med. Biol.*, vol. 41, no. 41, pp. 2251–2269, 1996.

[9] L. L. Wang *et al.*, "Assessment of alterations in the electrical impedance of muscle after experimental nerve injury via finite-element analysis," *IEEE Trans. Biomed. Eng.*, vol. 58, no. 6, pp. 1585–1591, Jun. 2011.

[10] M. Jafarpoor *et al.*, "Optimizing electrode configuration for electrical impedance measurements of muscle via the finite element method," *IEEE Trans. Biomed. Eng.*, vol. 60, no. 5, pp. 1446–1452, May 2013.

[11] S. B. Rutkove, A. Pacheck, and B. Sanchez, "Sensitivity distribution simulations of surface electrode configurations for electrical impedance myography," *Muscle Nerve*, vol. 56, no. 5, pp. 887–895, 2017.

[12] D. Li *et al.*, "Analysis of electrical impedance myography electrodes configuration for local muscle fatigue evaluation based on finite element method," *IEEE Access*, vol. 8, pp. 172 233–172243, 2020.

[13] L. K. Huang *et al.*, "Electrical impedance myography applied to monitoring of muscle fatigue during dynamic contractions," *IEEE Access*, vol. 8, pp. 13056–130 65, 2020.

[14] E. T. McAdams and J. Jossinet, "Tissue impedance: A historical overview," *Physiol. Meas.*, vol. 16, no. 3 A, pp. A1–A13, Aug. 1995.

[15] X. Luo, S. Wang, and B. Sanchez, "A framework for modeling bioimpedance measurements of nonhomogeneous tissues: A theoretical and simulation study," *Physiol. Meas.*, vol. 42, no. 5, 2021, Art. no. 055007.

[16] Imaios, "E-anatomy the interactive atlas of human anatomy," 2020. [Online]. Available: https://doi.org/10.37019/e-anatomy

[17] S. Hyem and A. Mokhtar, "Modeling for surface biopotential recording : Impedance measurements and noise," in *Proc. IEEE 2nd Int. Conf. Adv. Biomed. Eng.*, 2013, pp. 49–52.

[18] F. J. Pettersen and J. O. Høgetveit, "From 3D tissue data to impedance using simpleware ScanFE IP and COMSOL multiphysics - A tutorial," *J. Electr. Bioimpedance*, vol. 2, no. 1, pp. 13–32, 2011.

[19] S. Grimnes and Ø. G. Martinsen, "Cole electrical impedance model - A critique and an alternative," *IEEE Trans. Biomed. Eng.*, vol. 52, no. 1, pp. 132–135, Jan. 2005.

[20] S. Rodriguez *et al.*, "A batteryless sensor ASIC for implantable bioimpedance applications," *IEEE Trans. Biomed. Circuits Syst.*, vol. 10, no. 3, pp. 533–544, Jun. 2016.

[21] A. D. F. Schrunder, "Complete project repository of finite element analysis, circuit modelling, and measurement results," 2021. [Online]. Available: https://github.com/aledafers/FEA_CircuitSim_Methdology_EIM_Limbs

[22] G. J. Esper *et al.*, "Assessing neuromuscular disease with multifrequency electrical impedance myography," *Muscle Nerve*, vol. 34, no. 5, pp. 595–602, 2006.

[23] S. B. Rutkove, P. M. Fogerson, L. P. Garmirian, and A. W. Tarulli, "Reference values for 50-kHZ electrical impedance myography," *Muscle Nerve*, vol. 38, no. 3, pp. 1128–1132, 2008.

[24] J. Sandby-Møller, T. Poulsen, and H. C. Wulf, "Epidermal thickness at different body sites: Relationship to age, gender, pigmentation, blood content, skin type and smoking habits," *Acta Derm. Venereol.*, vol. 83, no. 6, pp. 410–413, 2003.